

Tuning the resistive switching properties of TiO₂-x films

N. Ghenzi, M. J. Rozenberg, R. Llopis, P. Levy, L. E. Hueso, and P. Stolar

Citation: *Applied Physics Letters* **106**, 123509 (2015); doi: 10.1063/1.4916516

View online: <http://dx.doi.org/10.1063/1.4916516>

View Table of Contents: <http://scitation.aip.org/content/aip/journal/apl/106/12?ver=pdfcov>

Published by the AIP Publishing

Articles you may be interested in

Improvement of resistive switching performances via an amorphous ZrO₂ layer formation in TiO₂-based forming-free resistive random access memory

J. Appl. Phys. **116**, 124514 (2014); 10.1063/1.4896402

Mechanism of localized electrical conduction at the onset of electroforming in TiO₂ based resistive switching devices

Appl. Phys. Lett. **104**, 113510 (2014); 10.1063/1.4869230

Influence of oxygen content of room temperature TiO₂-x deposited films for enhanced resistive switching memory performance

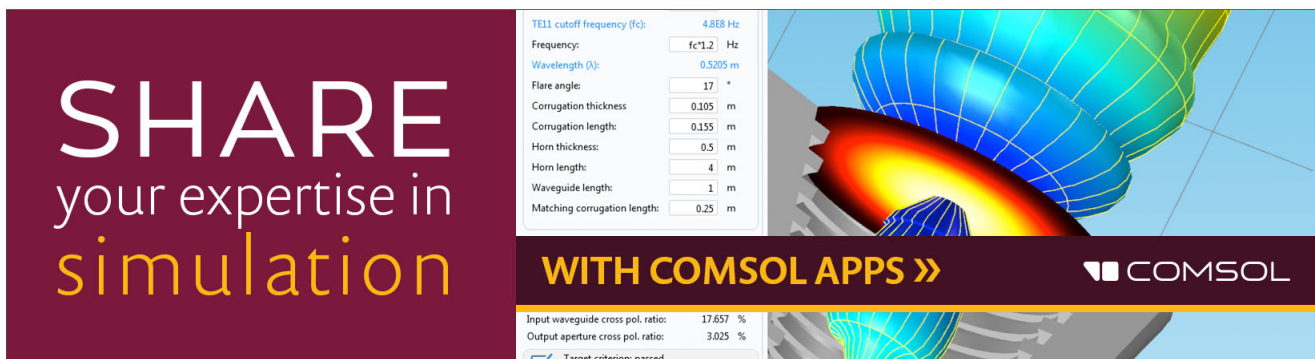
J. Appl. Phys. **115**, 034516 (2014); 10.1063/1.4862797

Role of oxygen vacancies in TiO₂-based resistive switches

J. Appl. Phys. **113**, 033707 (2013); 10.1063/1.4779767

Optical properties of Mg O – Ti O 2 amorphous composite films

J. Appl. Phys. **102**, 013520 (2007); 10.1063/1.2752118



SHARE your expertise in simulation

WITH COMSOL APPS »

COMSOL

TE11 cutoff frequency (fc): 4.8E8 Hz
Frequency: fc*1.2 Hz
Wavelength (λ): 0.5205 m
Flare angle: 17 °
Corrugation thickness: 0.105 m
Corrugation length: 0.155 m
Horn thickness: 0.5 m
Horn length: 4 m
Waveguide length: 1 m
Matching corrugation length: 0.25 m

Input waveguide cross pol. ratio: 17.657 %
Output aperture cross pol. ratio: 3.025 %
Target criterion: passed

Tuning the resistive switching properties of TiO_{2-x} films

N. Ghenzi,^{1,2,3} M. J. Rozenberg,^{4,5} R. Llopis,³ P. Levy,^{1,6} L. E. Hueso,^{3,7} and P. Stolarz^{2,3}

¹GAIANN, Centro Atómico Constituyentes, Comisión Nacional de Energía Atómica, Buenos Aires, Argentina

²ECyT, Universidad Nacional de San Martín, Campus Miguelete, 1650 San Martín, Argentina

³CIC nanogUNE, 20018 Donostia-San Sebastián, Basque Country, Spain

⁴Laboratoire de Physique des Solides, UMR8502, Université Paris-Sud, Orsay 91405, France

⁵Departamento de Física Juan José Giambiagi, FCEN, UBA, Buenos Aires, Argentina

⁶CONICET, Consejo Nacional de Investigaciones Científicas y Técnicas, Buenos Aires, Argentina

⁷IKERBASQUE, Basque Foundation for Science, 48011 Bilbao, Basque Country, Spain

(Received 31 January 2015; accepted 18 March 2015; published online 27 March 2015)

We study the electrical characteristics of TiO_{2-x} -based resistive switching devices fabricated with different oxygen/argon flow ratio during the oxide thin film sputtering deposition. Upon minute changes in this fabrication parameter, three qualitatively different device characteristics were accessed in the same system, namely, standard bipolar resistive switching, electroforming-free devices, and devices with multi-step breakdown. We propose that small variations in the oxygen/argon flow ratio result in relevant changes of the oxygen vacancy concentration, which is the key parameter determining the resistive switching behavior. The coexistence of percolative or non-percolative conductive filaments is also discussed. Finally, the hypothesis is verified by means of the temperature dependence of the devices in low resistance state. © 2015 AIP Publishing LLC.

[<http://dx.doi.org/10.1063/1.4916516>]

Resistive switching (RS) is emerging as key physical mechanism for the next generation of nonvolatile memory devices.¹ RS-based devices are fabricated as metal-insulator-metal (MIM) structures where the insulator resistance is controlled by electrical pulses.^{2–4} Several physical mechanisms have been suggested for the development of RS devices; Mott transition,⁵ Schottky barrier behavior at the interface,⁶ charge trapping,⁷ electric field-induced generation of crystalline defects,⁸ and oxygen vacancy diffusion.⁹ In RS devices, a SET process leads to a low resistance state (LR). The complementary process, referred as RESET, results in a high resistance state (HR). Remarkably, these two processes can be repeated a large number of times, with good reproducibility, enabling the implementation of non-volatile memory devices. In many cases, the electrical requirements for the first SET in a pristine device are very different from the subsequent SET pulses. This electrical initialization is called the electroforming process.

Operational reliability, in terms of uniformity in the switching current-voltage (I-V) response and good endurance characteristics, is one of the key areas of current research in RS-based memory devices.^{10,11} Nowadays, it is widely accepted that fine tuning of growth conditions and an electroforming protocol largely determine the operational response of the devices.¹² Nevertheless, often happens that seemingly similar devices present radically different RS characteristics. For example, a very broad range of characteristics have been reported in MIM structures based on TiO_{2-x} films, ranging from electroforming-free devices to systems requiring high forming voltages and non-uniform switching characteristics.¹⁰ Thus, the present work is focused on titanium-oxide-based devices, and we shall systematically investigate the dependence of the resulting RS characteristics with growth conditions of the insulating film.

Specifically, we study how different oxygen/argon flow ratio during the sputtering affects the response of the device. Among our main results, we find that we may tune between different RS characteristics by minute changes in this fabrication parameter. The underlying processes behind this behavior are discussed as well. In this context, our study contributes to the understanding of the relevance of oxide characteristics that define the very first relevant step in the response of the device.

Titanium oxide is emerging as one of the main materials in the development of RS memories.¹³ Furthermore, the physics of titanium oxides is relatively well understood, including, in particular, the properties of the oxide as a function of the oxygen defect density.^{14,15} Similar to a wide variety of resistive switching materials, titanium oxides also show uncontrolled phase transition from the insulating pristine phase (rutile and anatase) to the conductive Magneli or metallic phases.^{16–18} In these phase transitions, the re-ordering and creation of defects to switch between the different available phases is still under discussion.^{19,20} Due to that the understanding as the density of pre-existing defects and the oxide phase (determined mainly by the growth conditions) play a crucial role in the subsequent RS response.^{21–23}

We have made cross-shaped $\text{Ti}(45\text{ nm})/\text{TiO}_2(7\text{ nm})/\text{Pd}(25\text{ nm})$ structures with area ranging from $10^3 \mu\text{m}^2$ to $10^5 \mu\text{m}^2$ (see bottom inset of Fig. 1). TiO_2 films were grown by reactive sputtering with a pressure of 7 mTorr and a power of 200 W at room temperature.¹⁸ The sputtering gun is located in a 4Wave ion miller with a Ti target. Oxygen was injected in the chamber near to the target. We changed the oxygen/argon flow ratio between 25% and 37%. The bottom (BE) and top (TE) electrodes were deposited by DC sputtering and patterned by photolithography. We use Pd top electrode, which has a work function of 5.12 eV, what results in the formation of a Schottky barrier in the $\text{Pd}/\text{TiO}_{2-x}$

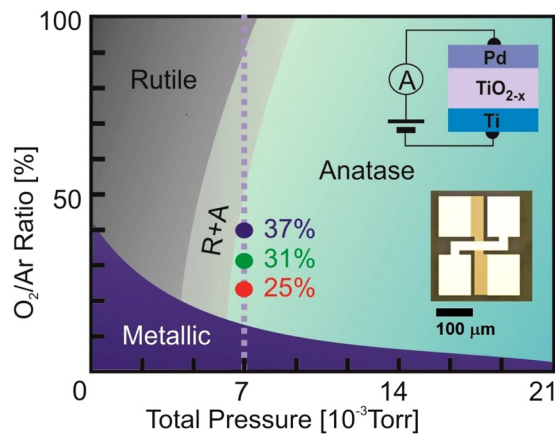


FIG. 1. Schematic oxygen/argon flow ratio ($x_{O_2/Ar}$) as a function of the total pressure phase diagram of TiO_x indicating the more stable structural phase. Reprinted with permission from P. Zeman and S. Takabayashi, Surf. Coat. Technol. **153**, 93 (2002). Copyright 2002 Elsevier. Top inset: Schematic device. Bottom inset: Optical image in the top view of the device.

interface. Ti bottom electrode results in an ohmic contact in the Ti/TiO_{2-x} interface.

Fig. 1 shows the phase diagram of the TiO_{2-x} structural phase as a function of the total pressure (p_{tot}) and the oxygen/argon flow ratio ($x_{O_2/Ar} = Q_{O_2}/Q_{Ar}$, with Q_{O_2} and Q_{Ar} the flow of oxygen and argon injected in the chamber) during the sputtering deposition.^{18,24,25} The three different flow ratios ($x_{O_2/Ar} = 25\%$, 31% , and 37%) adopted here are indicated in the diagram. The TiO_{2-x} films presented anatase-predominant nanocrystal phase in the three cases, as confirmed by ellipsometry and X-ray measurements (results not shown here). With the change in $x_{O_2/Ar}$, we control the density of oxygen vacancies present in the TiO_{2-x} films.

In order to rationalize Fig. 1, we may think of the variation in the relative number of available ions (O, Ar, and Ti) with p_{tot} and $x_{O_2/Ar}$ inside the chamber during the sputtering deposition. Thus, metallic TiO_x (i.e., oxygen-vacancy rich) is obtained at low values of $x_{O_2/Ar}$ during the sputtering deposition. Insulating state (either rutile or anatase) is obtained at high values of P_{O_2} (i.e., few oxygen vacancies). The amount of oxygen ions (N_{O_2}) inside the deposition chamber is available to react with the sputtered Ti ions increases for a higher value of p_{tot} . This implies that the value of the flow ratio limit between the metallic and the insulating states decreases at a higher total pressure value, and scales inversely proportional to p_{tot} . In contrast, values of the flow ratio ($x_{O_2/Ar}$) higher than this limit pressure induce insulating states (either rutile or anatase phase). At low values of p_{tot} , the sputtered ions arrive to the substrate with a high energy value due to the small number of collisions with the sputtering gas ions inside the chamber.²⁶ This results in Ti and O atoms diffusing a considerable distance into the substrate once reached, which yields the phase of lower thermodynamic energy: rutile, see Ref. 27. At higher values of p_{tot} , the energy with which Ti and O ions reach the substrate decreases, so that the diffusion distance of the deposited ions in the surface of the substrate decreases. This yields the oxide phase with the higher thermodynamic energy: anatase.²⁷

Electrical characterizations of the devices were performed in a Everbeing 4 in. probe station in air with a

Keithley 2635A SMU (in the case of the RS measurements, see below) and in vacuum in a LakeShore probe station with a Keithley 4200 SCS (measurement in temperature). All the electrical measurements were performed with bottom electrode grounded. No dependence of the RS behavior on the device area was observed, ranging from $10^3 \mu m^2$ to $10^5 \mu m^2$, which is consistent with the filamentary mechanism. We followed a pulsing protocol that provides two kinds of measurement. Voltage ramps consisting of pulses (10 ms duration and 500 ms of separation) of increasing/decreasing amplitude with step 0.05 V were applied. These are the so called writing pulses. From the measurement of the current during these writing pulses, we constructed the dynamical I-V curves. The remnant (i.e., the non-volatile) two terminal resistance was also measured in between the writing pulses by means of a small and non-disturbing constant reading voltage of 0.1 V. Thus, from the remnant resistance values and the pulse strength one constructs the hysteresis switching loop (HSL).²⁸ Threshold voltages for SET and RESET processes are extracted from the HSL, i.e., the position of the transitions. Then, from the I-V curves we read the current required to SET or RESET the devices at the corresponding threshold voltages.

The hysteretic I-V and HSL curves of devices fabricated with 25%, 31%, and 37% oxygen partial pressure were measured. We show the results in Fig. 2. We first analyse the initial part of the data, starting from 0 V with a positive voltage sweep. The low currents observed in the I-V curves at low bias evidence the insulating nature of the titanium oxide in the three samples. However, the three devices presented different leakage current: 100 nA for $x_{O_2/Ar} = 25\%$, 5 nA for $x_{O_2/Ar} = 31\%$, and 250 pA for $x_{O_2/Ar} = 37\%$ at 0.1 V. This difference results from the different density of oxygen vacancies in the bulk of the titanium oxide. The oxygen vacancies act like dopants contributing with free electrons to

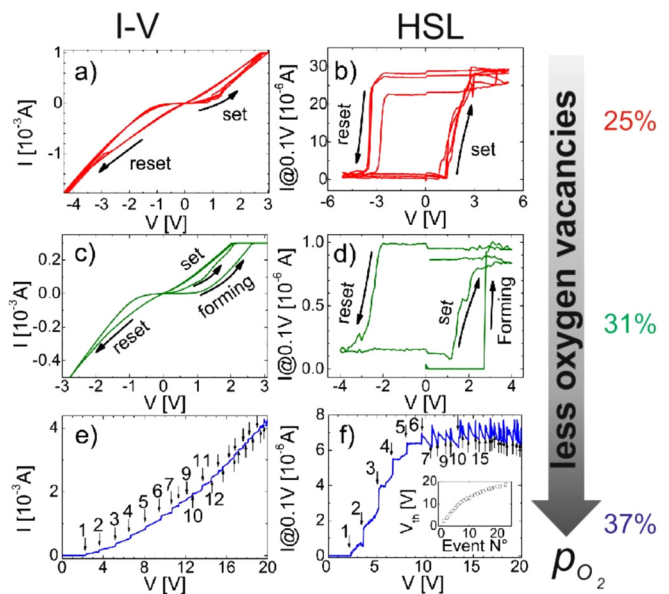


FIG. 2. I-V and HSL device characteristics of the sample with (a) and (b) $x_{O_2/Ar} = 25\%$, (c) and (d) $x_{O_2/Ar} = 31\%$, and (e) and (f) $x_{O_2/Ar} = 37\%$. Forming-free resistive switching characteristics are found in the sample with $p_{O_2} = 25\%$. After the electroforming process, the device is in the ON state of bipolar RS with $x_{O_2/Ar} = 31\%$. The $x_{O_2/Ar} = 37\%$ sample shows no RS response.

the conduction band of the oxide, what results in the titanium oxide behaving like an n-type semiconducting material.²⁹

As the voltage increases, this first sweep triggers the electroforming at an electric field close to the breakdown voltage in the second and third samples. In contrast, the first sample showed a sharp onset of conduction, but did not show an initial sudden electroforming event; hence, it is an electroforming-free device. The second sample showed a single sharp forming event, and the third one showed a succession of jumps. For the field values involved in the electroforming (10^7 V cm^{-1}), it is likely that oxygen ions and defects may move (or even be created) by a combined mechanism of drift and diffusion, as a consequence of the applied voltage and the local heating, respectively. We observe in the forming-free device (25% flow ratio sample) the sharp conduction onset voltage is around 1.2 V, switching from the pristine state to the LRS in a continuous way. In the 31% flow ratio sample, the forming voltage is around 2.7 V switching from the pristine state to the LR in an abrupt way. The 37% flow ratio sample shows no clear forming voltage but several transitions to a progressively increasing conductive state up to a maximum voltage of 20 V. Remarkably, negative electroforming procedure did not result in any stable resistive switching behavior, which indicates the inefficiency of the ohmic contact in the Ti/TiO_{2-x} bottom interface.

The next step after electroforming is to analyze the effect of cycling positive and negative voltage ramps. The protocol we follow is to apply the voltage ramps from 0 to 5 V, then decreasing down to -5 V, and finally returning to 0 V to complete one cycle. The ramps consist of discrete pulses with a step of 0.05 V. We set the current compliance I_{cc} at 1 mA for the samples with $x_{O_2/Ar} = 25\%$ and a value of 300 μA for the $x_{O_2/Ar} = 31\%$ samples to observe optimal bipolar RS (see description below). For the $x_{O_2/Ar} = 37\%$ samples, it was not possible to find any condition where RS appears, even after sweeping the applied voltage up to 20 V in both polarities with no current compliance.

As shown in the I-V curve of Fig. 2(a), two branches corresponding to the HR and LR states are present. These measurements exhibit the characteristic nonlinear behavior of the bipolar resistive switching mode. The fact that the applied current during the RESET process is similar to the current compliance in the SET process, 1 mA, is an indication of the bipolar nature of the resistive switching. In the same run, in between the discrete pulses we read the remnant resistance, and construct the HSL presented in Fig. 2(b). The remnant resistance exhibits two well-defined resistance values, the LR state around $R_{LR} = 3 \text{ k}\Omega$ and the HR state at $R_{HR} = 100 \text{ k}\Omega$ ($R_{HR}/R_{LR} = 30$), and two rapid transitions between them. Initially, the device is in the HR state. At about +1 V it switches to the LR state (SET transition) where it remains, until it switches back again to the HR state (RESET transition), at the negative polarity voltage of -3.2 V.

In Figs. 2(c) and 2(d), we show the I-V and HSL curve of the $x_{O_2/Ar} = 31\%$ sample. After the electroforming at a voltage of 2.5 V, two branches corresponding to HR and LR states appear, with good reproducibility and similar to the $x_{O_2/Ar} = 25\%$ sample. Indeed, SET and RESET voltages in both samples appear to be qualitatively similar. Nevertheless, the maximum current amplitude in the SET and RESET

process of the $x_{O_2/Ar} = 31\%$ case is approximately 400 μA , that is, 2.5 times smaller than the corresponding one in the $x_{O_2/Ar} = 25\%$ sample, which represents an improvement for eventual applications.

Figs. 2(e) and 2(f) present the I-V and HSL curve of the $x_{O_2/Ar} = 37\%$ sample. In this case, no RS response is observed but multiple current jumps appear. Initially, increments of $\sim 1 \text{ V}$ are required between consecutive jumps. This required voltage increment gets reduced as the number of jumps accumulates (see the inset of Fig. 2(f)).

It is nowadays widely accepted that the microscopic origin of the bipolar RS in TiO_{2-x} material is attributed to the migration of oxygen vacancies (OV) along nanometer regions close to the electrodes. The oxygen vacancy content in the active interface (Pd/TiO₂) determines the resistance value. Thus, the back and forth movement of oxygen ions of the Pd interface is the cause of the observed switching.^{21,22} Additionally, it is likely the formation of Pd-O bonding due to migration of oxygen towards the Pd electrode, giving like result the Pd electrode can act as a reservoir of oxygen ions. Through a fine control of the pre-existing OV content (due to the change in $x_{O_2/Ar}$) and the electroforming voltage procedure we are effectively controlling the size of the OV-based conductive filament (CF). In fact, we argue that a higher value of $x_{O_2/Ar}$ produces a smaller diameter size of the OV-based CF because a smaller density of vacancies is

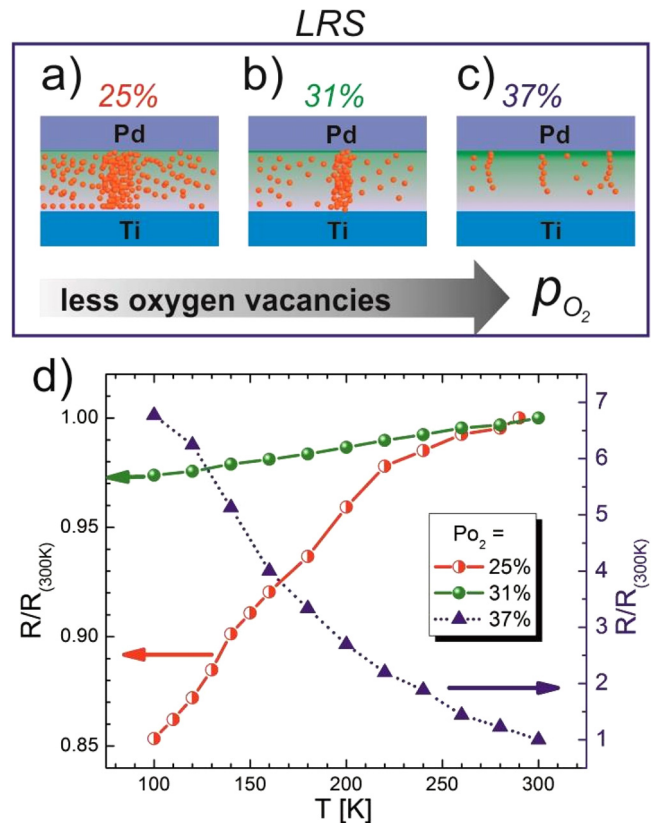


FIG. 3. Oxygen vacancies distribution in the LR state in the samples grown with $x_{O_2/Ar} = 25\%$ (a), $x_{O_2/Ar} = 31\%$ (b), and $x_{O_2/Ar} = 37\%$ (c) of oxygen/argon flow ratio. The oxygen vacancy density decreases when the flow ratio increases. This effect results in a lowering of the injection barrier in the Pd/TiO₂ interface. (d) Temperature dependence of the LR state in the three explored devices. To facilitate the comparison, we normalized the resistance with the room temperature value in all cases.

present in the material. The conceptual picture is sketched in Figs. 3(a)–3(c) for the three argon/oxygen flow ratios devices in the LR state. In the $x_{O_2/Ar} = 25\%$ sample, we expect the CF will be wider when compared to the CF corresponding to samples with less OV density. This is consistent with the high value of the applied current compliance (1 mA), resulting in a $3\text{ k}\Omega$ resistance value. As in the $x_{O_2/Ar} = 31\%$ sample the OV density is reduced, the size of the CF is smaller, which results in a larger $100\text{ k}\Omega$ resistance value. In these two cases, the current predominantly flows within the CF region. In the $x_{O_2/Ar} = 37\%$ sample, the richer oxygen atmosphere possibly prevents the formation of filaments, and the conduction most likely takes place along grain boundaries and dislocations (as we shall see later by the dependence with temperature). It results in a higher resistance value in the order of $500\text{ k}\Omega$ for $V = 4\text{ V}$ (maximum applied voltage in the other cases), as seen in Fig. 2(f).

In order to provide further support to the qualitative picture of CF formation, we measured the temperature dependence of the samples between 100 K and 300 K. We show the results for the three cases in Fig. 3(d). The two samples that show RS were measured in the LR state. The resistance values at room temperature are $3\text{ k}\Omega$, $100\text{ k}\Omega$, and $15\text{ k}\Omega$ for the $x_{O_2/Ar} = 25\%$, 31% , and 37% , respectively.

For the $x_{O_2/Ar} = 25\%$ and 31% samples, the resistance shows a metallic character while for the $x_{O_2/Ar} = 37\%$ sample it shows a semiconducting behavior (see Fig. 3(d)). The observed metallic behavior is in line with the hypothesis of the formation of a percolative conductive filament originated by the diffusion of oxygen vacancies through the insulating matrix. Nonetheless, the change in the resistance is only $\Delta R_{LR} = 16\%$ and $\Delta R_{LR} = 2\%$ for the $x_{O_2/Ar} = 25\%$ and 31% sample, respectively, indicating that the conduction in the filaments is very poorly metallic, and likely dominated by disorder. Due to the observed resistance variation, we expect the CF is in a metallic phase (Ti rich). In contrast, the semiconducting behavior for the $x_{O_2/Ar} = 37\%$ sample as well as the existence of multiple jumps in the current response indicate the likely presence of non-percolating filamentary structures through the oxide thin film. The difference between both types of behavior indicates that there is a critical flow ratio where two different modes appear: percolative or non-percolative CF generation.

In conclusion, a wide range of behavior has been reported in TiO_2 -based devices, namely, forming-free, sharp forming, and no resistive switching at all (TiO_2 free-forming devices,^{13,30} control of the forming voltage,^{10,16} multiple current jumps associated with different driving modes^{31,32}). Here, we show that all these behaviors may be present in the same system. We found that the critical parameter which actually determines the characteristics of the device is the oxygen/argon flow ratio at the time of the active layer fabrication. It allowed us to obtain these three qualitatively different behaviors, which in turn, can be related to the temperature dependence of the conductive filaments. Our results suggest that this control can be directly associated to different oxygen vacancy concentrations, which is modulated by the oxygen/argon flow ratio during the film deposition. Indeed, a critical value of the oxygen/argon flow ratio that delimits the transition between a single or multiple channel mode was found. Finally, the validation of the proposed

image by the temperature dependence of the LR state opens the way for a rapid testing of different configurations of current channels. An interesting question that we leave for future study is the possible correlation of fabrication condition with the endurance of the devices.

We acknowledge the support of the Spanish Ministry of Economy through the Ramon y Cajal (RYC-2012-01031) program, PIP MeMO, and PICT MeMOSat (CONICET, Argentina).

- ¹R. Waser, R. Dittmann, G. Staikov, and K. Szot, *Adv. Mater.* **21**, 2632 (2009).
- ²G. I. Meijer, *Science* **319**, 1625 (2008).
- ³M. Rozenberg, *Scholarpedia* **6**, 11414 (2011).
- ⁴A. Sawa, *Mater. Today* **11**, 28 (2008).
- ⁵R. Fors, S. I. Khartsev, and A. M. Grishin, *Phys. Rev. B* **71**, 045305 (2005); T. Oka and N. Nagaosa, *Phys. Rev. Lett.* **95**, 266403 (2005).
- ⁶T. Fujii, M. Kawasaki, A. Sawa, H. Akoh, Y. Kawazoe, and Y. Tokura, *Appl. Phys. Lett.* **86**, 12107 (2005).
- ⁷M. J. Rozenberg, I. H. Inoue, and M. J. Sanchez, *Phys. Rev. Lett.* **92**, 178302 (2004).
- ⁸S. Tsui, Y. Q. Wang, Y. Y. Xue, and C. W. Chu, *Appl. Phys. Lett.* **89**, 123502 (2006); M. Hamaguchi, K. Aoyama, S. Asanuma, Y. Ues, and T. Katsufuji, *ibid.* **88**, 142508 (2006).
- ⁹M. Quintero, P. Levy, A. G. Leyva, and M. J. Rozenberg, *Phys. Rev. Lett.* **98**, 116601 (2007).
- ¹⁰J. J. Yang, I. H. Inoue, T. Mikolajicka, and C. S. Hwang, *MRS Bull.* **37**, 131 (2012).
- ¹¹N. Ghenzi, M. J. Snchez, M. J. Rozenberg, P. Stolar, F. G. Marlasca, D. Rubi, and P. Levy, *J. Appl. Phys.* **111**, 084512 (2012).
- ¹²S. J. Song, J. Y. Seok, J. H. Yoon, K. M. Kim, G. H. Kim, M. H. Lee, and C. S. Hwang, *Sci. Rep.* **3**, 3443 (2013).
- ¹³D. B. Strukov, G. S. Snider, D. R. Stewart, and R. S. Williams, *Nature* **453**, 80 (2008).
- ¹⁴K. A. Bogle, M. N. Bachhav, M. S. Deo, N. Valanoor, and S. B. Ogale, *Appl. Phys. Lett.* **95**, 203502 (2009).
- ¹⁵I. Salaoru, T. Prodromakis, A. Khiat, and C. Toumazou, *Appl. Phys. Lett.* **102**, 013506 (2013).
- ¹⁶D. S. Jeong, H. Schroeder, and R. Waser, *Phys. Rev. B* **79**, 195317 (2009).
- ¹⁷V. Guiot, L. Cario, E. Janod, B. Corraze, V. T. Phuoc, M. J. Rozenberg, P. Stolar, T. Cren, and D. Roditchev, *Nat. Commun.* **4**, 1722 (2013).
- ¹⁸N. Ghenzi, D. Rubi, E. Mangano, G. Giménez, P. Stolar, and P. Levy, *Thin Solid Films* **550**, 683 (2014).
- ¹⁹S. M. Sze and G. Gibbons, *Appl. Phys. Lett.* **8**, 111 (1966).
- ²⁰J. Blasco, N. Ghenzi, J. Sue, P. Levy, and E. Miranda, *IEEE Electron Device Lett.* **35**, 390 (2014).
- ²¹J. J. Yang, D. B. Strukov, and D. R. Stewart, *Nat. Nanotechnol.* **8**, 13 (2013).
- ²²N. Ghenzi, M. J. Sánchez, and P. Levy, *J. Phys. D: Appl. Phys.* **46**, 415101 (2013).
- ²³N. Ghenzi, M. J. Sánchez, D. Rubi, M. J. Rozenberg, C. Urdaniz, M. Weissman, and P. Levy, *Appl. Phys. Lett.* **104**, 183505 (2014).
- ²⁴S. D. Shang, S. J. Rong, S. B. Gen, and W. Matthias, *Chin. Phys. B* **22**, 67202 (2013).
- ²⁵“Effect of total and oxygen partial pressures on structure of photocatalytic TiO_2 films sputtered on unheated substrate,” Fig. 1 of P. Zeman and S. Takabayashi, *Surf. Coat. Technol.* **153**, 93 (2002).
- ²⁶J. H. Lee, G. Luo, I. C. Tung, S. H. Chang, Z. Luo, M. Malshe, M. Gadre, A. Bhattacharya, S. M. Nakmans, J. A. Eastman *et al.*, *Nat. Mater.* **13**, 879 (2014).
- ²⁷D. Hanaor and C. Sorrell, *J. Mater. Sci.* **46**, 855 (2011).
- ²⁸N. Ghenzi, M. J. Sánchez, F. G. Marlasca, P. Levy, and M. Rozenberg, *J. Appl. Phys.* **107**, 093719 (2010).
- ²⁹N. Ghenzi, P. Stolar, M. C. Fuertes, F. G. Marlasca, and P. Levy, *Phys. B* **407**, 3096 (2012).
- ³⁰C. Hermes, R. Bruchhaus, and R. Waser, *IEEE Electron Device Lett.* **32**, 1588 (2011).
- ³¹C. Hu, M. D. McDaniel, J. G. Ekerdt, and E. T. Yu, *IEEE Electron Devices Lett.* **34**, 1385 (2013).
- ³²C. Hu, M. D. McDaniel, A. Posadas, A. A. Demkov, J. G. Ekerdt, and E. T. Yu, *Nano Lett.* **14**, 4360 (2014).